J. Fluid Mech. (2001), *vol.* 448, *pp.* 213–241.
DOI: 10.1017/S0022112001005948 Printed in the United Kingdom

The first effects of fluid inertia on flows in ordered and random arrays of spheres

By REGHAN J. HILL[1], DONALD L. KOCH[1] AND ANTHONY J. C. LADD[2]

[1]School of Chemical Engineering, Cornell University, Ithaca, NY 14853, USA
[2]Department of Chemical Engineering, University of Florida, Gainesville, FL 32611, USA

(Received 3 January 2001 and in revised form 4 June 2001)

Theory and lattice-Boltzmann simulations are used to examine the effects of fluid inertia, at small Reynolds numbers, on flows in simple cubic, face-centred cubic and random arrays of spheres. The drag force on the spheres, and hence the permeability of the arrays, is determined at small but finite Reynolds numbers, at solid volume fractions up to the close-packed limits of the arrays. For small solid volume fraction, the simulations are compared to theory, showing that the first inertial contribution to the drag force, when scaled with the Stokes drag force on a single sphere in an unbounded fluid, is proportional to the square of the Reynolds number. The simulations show that this scaling persists at solid volume fractions up to the close-packed limits of the arrays, and that the first inertial contribution to the drag force relative to the Stokes-flow drag force decreases with increasing solid volume fraction. The temporal evolution of the spatially averaged velocity and the drag force is examined when the fluid is accelerated from rest by a constant average pressure gradient toward a steady Stokes flow. Theory for the short- and long-time behaviour is in good agreement with simulations, showing that the unsteady force is dominated by quasi-steady drag and added-mass forces. The short- and long-time added-mass coefficients are obtained from potential-flow and quasi-steady viscous-flow approximations, respectively.

1. Introduction

There exists a large body of theoretical and experimental studies of Stokes flows in porous media, i.e. flows for which the Reynolds number is assumed to be identically zero. However, in many industrial applications, high fluid velocities are required to achieve adequate rates of heat and mass transfer. Consequently, Reynolds numbers from practically zero up to $O(10^4)$ are encountered in practice (Perry & Green 1984). Typical industrial applications include packed-bed reactors, absorption columns and filters.

To bridge the gap between the existing knowledge of steady Stokes flows in porous media and the moderate-Reynolds-number flows addressed in the accompanying paper (Hill, Koch & Ladd 2001), we consider two types of flows that depend on the effects of fluid inertia at small Reynolds numbers. In one, the transient development of flows whose Reynolds numbers are practically zero is considered, and in the other, steady flows with small but finite Reynolds numbers are examined. The lattice-Boltzmann method is used to compute the fluid velocity and the drag force on the

spheres in both ordered and random arrays, and the simulation results are compared to theoretical predictions for small Reynolds numbers and solid volume fractions.

The monodisperse arrays of spheres considered in this work have a solid volume fraction $c = n(4/3)\pi a^3$, where n is the sphere number density and a is the sphere radius. The Reynolds number is $Re = |\langle \boldsymbol{u} \rangle| a/\nu$, where $\langle \boldsymbol{u} \rangle$ is the spatially averaged velocity and ν is the fluid kinematic viscosity. Under steady-state conditions, the average pressure gradient driving the flow is balanced by the force density exerted by the spheres on the fluid, and hence $\langle \nabla p \rangle = n \langle \boldsymbol{f} \rangle$, where $\langle \boldsymbol{f} \rangle$ is the average drag force on the spheres. It is appropriate to non-dimensionalize the drag force with the magnitude of the Stokes-flow drag force on a single sphere in an unbounded fluid. Consequently, the non-dimensional drag force is defined as $F = |\langle \boldsymbol{f} \rangle|/(6\pi\mu a|\langle \boldsymbol{u} \rangle|)$, where μ is the fluid dynamic viscosity. For Stokes flows, F depends only on the sphere configuration and the solid volume fraction, whereas at finite Reynolds numbers it also depends on the Reynolds number and, for ordered arrays, the direction of the average pressure gradient relative to the axes of the arrays.

Our motivation for examining fixed beds of spheres with solid volume fractions considerably less than the close-packed limit comes from possible applications of the results to sedimenting suspensions. Koch (1990) argued that the velocity of the solids in large-Stokes-number gas–solid suspensions changes slowly relative to the viscous diffusion of momentum in the fluid, and hence the fluid velocity is similar to that in fixed beds. The Stokes number, which characterizes the ratio of particle inertia forces to viscous drag forces, is $St = Ua\rho_s/\mu$, where U is the average velocity of the particles relative to the fluid and ρ_s is the solid density. In addition to predicting the sedimentation velocity, Koch & Sangani (1999) showed that the Stokes-flow drag force on the spheres in fixed random arrays can be used to examine the stability of gas-fluidized beds, and hence the results of this work will contribute toward understanding how fluid inertia affects the stability of finite-Reynolds-number suspensions.

Numerical simulations have helped to elucidate the effects of fluid inertia on flows in *two-dimensional* porous media (Rojas & Koplik 1998; Andrade *et al.* 1997; Ghaddar 1995; Edwards *et al.* 1990; Eidsath *et al.* 1983). Koch & Ladd (1997) used theory and lattice-Boltzmann simulations to show how the drag force on the cylinders in square and random arrays depends on the Reynolds number, solid volume fraction and, for ordered arrays, the direction of the flow relative to the axis of the arrays. Simulations were performed at Reynolds numbers up to and exceeding the transition to unsteady flow.

Mei & Auriault (1991), using the methods of homogenization and multiple scales, predicted that the first inertial contribution to the Stokes-flow drag force (per unit volume) should increase with the cube of the average fluid velocity, i.e. that the inertial contribution to F should be proportional to Re^2, but their theory was sufficiently general so as not to predict the dependence of the drag force on the solid volume fraction for any specific geometry, although this could, in principle, be obtained by solving the averaged equations resulting from their theory. It is interesting to note that this scaling has not yet been corroborated experimentally, presumably because the range of Reynolds numbers where it occurs is very small. Furthermore, as noted by Mei & Auriault, the inertial contribution to the drag force is small relative to the Stokes-flow drag force, and hence it would be difficult to measure.

Some experimental verification of the Re^2 dependence of the inertial contribution to F may be obtained from the experiments of Fand *et al.* (1987), who measured the permeability of a cylindrical packed bed of approximately monodisperse glass spheres. The solid volume fraction was 0.643, the radius of the cylinder was $40a$,

and Reynolds numbers up to approximately 200 were achieved. Their results suggest that $F = 151$ when $Re < 1$, and $F = 145 + 4.70Re$ when $2.5 < Re < 40$. However, if we assume that there is a transition from Re^2 to Re scaling, and we require the F and $\partial F/\partial Re$ to be continuous there, then these results suggest that $F = 151 + 0.92Re^2$ when $Re < 2.6$. This shows that the first inertial contribution to F, being less than 2% of the Stokes-flow drag force, is indeed very small and, hence, difficult to measure. The simulations performed in this work provide an excellent means of determining the range of Reynolds numbers where Re^2 scaling occurs, and how this range depends on the solid volume fraction. Note that the linear dependence of F on Re, which occurs at larger Reynolds numbers, is addressed in the accompanying paper (Hill *et al.* 2001).

Cheng & Papenicolaou (1997) recently proposed a theory for the first inertial contribution to the drag force on the spheres in dilute simple cubic arrays. In the limit of the Reynolds number based on the sphere separation, $Re_L = ReL/a = 4\pi Re/(3c)^{1/3}$, vanishing, their tabulated results suggest that $F = 1.77c^{1/3} + 0.333Re$. This is approximately the same as the $O(c^{1/3})$ theory of Hasimoto (1959) for Stokes flows in dilute simple cubic arrays of spheres, but with an inertial correction proportional to the Reynolds number. This scaling contradicts the theory of Mei & Auriault (1991) and the theory and simulations of Koch & Ladd (1997), which show that the first inertial contribution to F should be proportional to Re^2.

By expanding the velocity and the pressure as power series in the Reynolds number, Koch & Ladd (1997) showed that the $O(Re)$ contribution to F must vanish, because the $O(Re)$ contributions to the velocity and the pressure must be odd and even functions of position, respectively. They showed that the $O(Re^2)$ contributions to the velocity and the pressure must be even and odd functions of position, respectively, and hence that the first inertial contribution to F must be $O(Re^2)$. While these arguments also apply to cubic arrays of spheres, quantitative results were derived specifically for two-dimensional arrays of aligned cylinders.

Therefore, in § 6.1, we develop a theory for the first inertial contribution to F, for dilute simple cubic arrays of spheres, which has the expected dependence on the Reynolds number. The fundamental periodic solution of the Oseen equations is matched to the solution of the Stokes equations for flow past a single sphere in an unbounded fluid. Quantitative comparisons of the theory and lattice-Boltzmann simulations are made, for the predicted dependence of the drag force on the solid volume fraction and the flow direction relative to the axes of the arrays.

For dilute random arrays of spheres, Kaneda (1986) calculated the first inertial contribution to the drag force by including the Oseen approximation of the inertial term in the Brinkman equations (Brinkman 1947). The asymptotic limits of his theory are

$$F \sim 1 + (3/\sqrt{2})c^{1/2} + (\sqrt{2}/40)c^{-1/2}Re^2 \quad (Re \ll c^{1/2} \ll 1) \tag{1}$$

and

$$F \sim 1 + (3/8)Re + (27/4)cRe^{-1} \quad (c^{1/2} \ll Re \ll 1). \tag{2}$$

Note that Kaneda's theory is extremely difficult to verify experimentally, because the solid volume fraction and the Reynolds number are both required to be small. Therefore, in § 6.3, we use lattice-Boltzmann simulations to determine the range of solid volume fractions where Kaneda's theory (1) is accurate. The simulations also extend the theory to give the coefficient of the $O(Re^2)$ inertial contribution to F at solid volume fractions up to the close-packed limit.

The effects of fluid inertia, at zero Reynolds number, are also examined by com-

paring theory and simulations for the transient in which the fluid is accelerated from rest toward a steady Stokes flow. Theoretical and computational methods typically used for calculating Stokes flows in porous media – boundary-integral and multipole methods, for example – are usually limited to steady flows. The lattice-Boltzmann method, however, requires that a steady-state be obtained by computing the temporal evolution of the fluid velocity. The fluid is typically accelerated from rest by applying a constant body force or average pressure gradient. In such cases, inertial effects are important – even when the Reynolds number is practically zero.

In § 5, we develop a theory for the short- and long-time temporal evolution of the spatially averaged velocity and drag force on the spheres in fixed arrays. The concepts of added mass and quasi-steady drag are used to predict the long-time evolution of the drag force from knowledge of the steady-state drag force and velocity variance, both of which are obtained for ordered and random arrays of spheres at solid volume fractions up to their close-packed limits.

Before presenting the results, the lattice-Boltzmann method and our simulation methodology are outlined in §§ 2 and 3, respectively. Lattice-Boltzmann simulations are first compared to existing theory and computations for steady Stokes flows in ordered and random arrays of spheres. The Stokes flow drag force and conditionally averaged velocity are presented in § 4. The effects of fluid inertia for unsteady zero-Reynolds-number flows are examined in § 5, followed by steady flows with small but finite Reynolds numbers in § 6. Within each section, results for ordered arrays are followed by those for random arrays. A summary follows in § 7.

2. The lattice-Boltzmann method

The lattice-Boltzmann method used in this work is discussed in detail by Ladd (1994*a*, *b*), and hence only a brief description is given here. Numerous applications of it, including references to its development from lattice-gas automata, can be found in the review by Chen & Dollen (1998) and in the book by Rothman & Zaleski (1997).

Solutions of the incompressible Navier–Stokes equations are obtained from the moments of a discretized fluid–particle velocity distribution function. There are 18 fluid–particle population densities at each node of a cubic lattice that extends throughout the computational domain. The population densities correspond to velocities in the directions to the 6 nearest and 12 next-nearest neighbouring lattice nodes. At each time step, the population densities are updated by performing collision and streaming steps, which relax the fluid–particle velocity distribution function toward equilibrium, and in doing so reproduce the incompressible Navier–Stokes equations on macroscopic length and time scales. The pressure and velocity are obtained from the zeroth and first moments of the fluid–particle velocity distribution function and the equation of state relating the density to the pressure. Compressibility errors are of the order of the Mach number squared, which can be kept small while increasing the Reynolds number by either decreasing the fluid viscosity or increasing the ratio of the sphere radius to the lattice-node spacing.

Boundary nodes, which represent the surface of the spheres, are placed halfway along the links between the lattice nodes that intersect the sphere surfaces. To ensure that the fluid velocity is zero at the sphere surfaces, the fluid–particle population densities are propagated in the opposite direction from which they approach the boundary nodes. The hydrodynamic drag force on the spheres is calculated by summing the impulses exerted on the spheres by the fluid particles. As a result of the cubic lattice, the spheres are not exactly spherical, and therefore an effective hydrodynamic radius must be defined. This is obtained by finding the small correction

to the nominal sphere radii of $j + 0.5$ lattice units ($j = 0, 1, 2, \ldots$) required for the Stokes-flow drag force on the spheres in dilute simple cubic arrays to agree with the theories of Hasimoto (1959) and Sangani & Acrivos (1982). With the fluid kinematic viscosity equal to 0.01, and for spheres with their centres at lattice nodes, the effective hydrodynamic radii of spheres with nominal radii of 0.5, 1.5 and 2.5 lattice units are 0.734, 1.88 and 2.86 lattice units, respectively. The effective hydrodynamic radii of larger spheres are $j + 0.8$ lattice units ($j = 3, 4, 5, \ldots$). While this approach is entirely satisfactory for the computations in this work, since the particles are fixed with their centres at lattice nodes, a more sophisticated treatment of the boundary conditions, which removes the restriction for the boundary nodes to be halfway between lattice nodes, is given by Verberg & Ladd (2000).

3. Simulation methodology

The porous media considered in this work are fixed periodic arrays of impermeable spheres with solid volume fractions

$$c = n(4/3)\pi a^3 = n_s(4/3)\pi(a/L)^3, \tag{3}$$

where n is the sphere number density, a is the sphere radius, and n_s is the number of spheres enclosed in a typically cubic computational domain whose volume is L^3. For simple cubic and face-centred cubic arrays of spheres, $n_s = 1$ and 4, respectively. For random arrays of spheres, n_s must be sufficiently large to minimize artifacts and statistical fluctuations coming from the finite size of the computational domain. In practice, n_s is chosen to be large enough to avoid periodic artifacts, and statistical uncertainty is reduced by ensemble averaging the results from n_c random sphere configurations.

The pressure and fluid velocity are governed by the incompressible Navier–Stokes equations, with the no-slip boundary condition at the sphere surfaces and periodic boundary conditions at the bounds of the computational domain. The lattice-Boltzmann method described in the previous section is used to calculate the fluid velocity and the forces on the spheres. The fluid is typically accelerated from rest by a constant body force, which is equivalent to applying a constant average pressure gradient to the fluid.

The assumption of a uniform body force, or linear pressure gradient, is valid locally in a bulk porous medium in situations where the gradient of the ensemble-averaged velocity is much smaller than $|\langle \boldsymbol{u} \rangle|/a$. In general, this condition will be satisfied at distances further than an $O(1)$ number of particle diameters from bounding walls.

The Reynolds number is defined as

$$Re = |\langle \boldsymbol{u} \rangle| a/\nu, \tag{4}$$

where ν is the fluid kinematic viscosity and $\langle \boldsymbol{u} \rangle$ is the spatially averaged velocity, which includes the volume occupied by the spheres. Note that the average velocity in the space occupied by the fluid is $\langle \boldsymbol{u} \rangle/(1-c)$, and that $\langle \boldsymbol{u} \rangle$ is equivalent to the velocity measured in an experiment by dividing the volumetric flow rate of the fluid by the cross-sectional area of the packed bed.

At finite Reynolds numbers, the average velocity is not necessarily in the same direction as the average pressure gradient. In this work, flows are considered for which the applied body force is directed at an angle θ_p from the x-axis in the (x, y)-plane. For simple cubic and face-centred cubic arrays of spheres, the average velocity lies in the (x, y)-plane, but at an angle $\theta_u = \arctan(\langle u_y \rangle / \langle u_x \rangle)$ from the x-axis.

The non-dimensional drag force is defined as

$$F = |\langle \boldsymbol{f} \rangle|/(6\pi\mu a|\langle \boldsymbol{u} \rangle|), \tag{5}$$

where $\langle \boldsymbol{f} \rangle$ is the average drag force on the spheres. The denominator on the right-hand side of (5) is the Stokes drag force on a single sphere in an unbounded fluid. Therefore, positive deviations of F from unity indicate the contribution of hydrodynamic interactions (finite solid volume fraction) and fluid inertia (finite Reynolds number) to the magnitude of the average drag force.

At steady state, the average drag force multiplied by the sphere number density is equal to the applied average pressure gradient. From (3) and (5), it follows that the magnitude of the average pressure gradient is

$$|\langle \nabla p \rangle| = 9c\mu F|\langle \boldsymbol{u} \rangle|/(2a^2). \tag{6}$$

The random sphere configurations used to calculate ensemble averages were generated using a Monte-Carlo (MC) method, whereby n_s spheres are initially placed with their centres at randomly chosen lattice sites throughout the computational domain (initialization). The sphere radius, and hence the solid volume fraction, is increased by a prescribed increment after sequentially displacing each of the spheres one lattice unit in randomly chosen directions (swelling), provided that each displacement does not result in spheres overlapping. When the required sphere radius is achieved, the random displacements are continued, but without increasing the sphere radius, until a *hard-sphere* distribution is achieved (equilibration). For the relatively small numbers of spheres used in the configurations, typically 16–64 in this work, this approach is reliable at solid volume fractions up to approximately 0.5.

At larger solid volume fractions, the distribution of the angle between the vectors separating each sphere from its two nearest neighbours suggested that some random sphere configurations generated using the MC method had become ordered. Therefore, at the largest solid volume fractions, sphere configurations generated using the method of Zinchenko (1994) were used. Zinchenko's method generates sphere configurations for which the solid volume fraction is as close as possible to the close-packed limit of random arrays of spheres, approximately 0.64. This is achieved by computing the evolution of the positions of the spheres in a continuous network, while increasing the sphere radius and, hence, the solid volume fraction. The positions of the spheres are constrained by the requirement that each remains in contact with three neighbours. Depending on the number of spheres in the computational domain, solid volume fractions in the approximate range 0.58–0.63 could be obtained. To achieve smaller solid volume fractions, the sphere radius was first decreased and then MC equilibration steps were applied so that, if it was unhindered by its neighbours, each sphere would diffuse a distance comparable to the average sphere separation. This procedure was intended to randomize the configurations without allowing time for possible crystallization.

In this work, the ensemble average of a quantity α is calculated from

$$\langle \alpha \rangle = \frac{1}{n_c} \sum_{i=1}^{n_c} \alpha_i, \tag{7}$$

and the uncertainty in the estimated mean, which is referred to as the standard error, is calculated from

$$\Delta\alpha = \sqrt{\mathrm{var}(\alpha)/(n_c - 1)}, \tag{8}$$

where $\mathrm{var}(\alpha) = \langle (\alpha - \langle \alpha \rangle)^2 \rangle$ is the variance of α calculated assuming n_c degrees of

freedom. Note that the factor $(n_c - 1)$ in the denominator on the right-hand side of (8) corrects for the fact that there are actually $n_c - 1$ degrees of freedom, since the mean is used to calculate the variance (Bevington & Robinson 1992). This is important only when the number of random configurations used to calculate the ensemble average of α is small, which is typically the case.

Occasionally, as few as one or two random configurations were used to compute ensemble averages, particularly for computations requiring a large sphere radius and a large number of spheres in the computational domain. The statistical error calculated from such a small number of random configurations cannot be guaranteed to be sufficiently small. However, if the spheres in each random configuration are independent of one another, the standard error calculated from (8) is expected to be inversely proportional to $(n_s n_c)^{1/2}$, and hence the statistical variation coming from the small number of random configurations is expected to be small when n_s is large.

Very rarely, an outlying observation that was ostensibly far from the mean was discarded. With a relatively small number of random configurations, these outliers give an unfair weighting to the estimated mean and variance. Chauvenet's criterion was applied, which allows an outlier to be discarded if, assuming Gaussian statistics apply, the probability of an observation being further from the mean than the outlier in question multiplied by the number of random configurations is less than 0.5 (Bevington & Robinson 1992).

4. Steady flows with zero Reynolds number

In this section, steady Stokes flows in ordered and random arrays of spheres are examined. These results provide an excellent means of testing the accuracy of the lattice-Boltzmann method over a wide range of solid volume fractions and grid resolutions, since they can be compared to the existing theoretical and computational results in the literature. Consequently, they establish the minimum computational requirements – sphere radius and number of spheres in the random configurations, for example – for the subsequent simulations of finite-Reynolds-number flows presented in this and the accompanying paper (Hill *et al.* 2001).

4.1. *The drag force for ordered arrays*

From the linearity of the Stokes equations and symmetry considerations, the Stokes-flow drag force on the spheres in cubic arrays is independent of the direction of the average velocity, and hence the drag force only needs to be calculated for a single direction of the average pressure gradient. From the fundamental periodic solution of the Stokes equations, Hasimoto (1959) calculated the drag force on the spheres in dilute simple cubic, body-centred cubic and face-centred cubic arrays. For simple cubic arrays, the non-dimensional drag force is given by

$$F^{-1} = 1 - 1.7601c^{1/3} + c - 1.5593c^2 + O(c^{8/3}). \tag{9}$$

The $O(c^{1/3})$ correction to the drag force on a single sphere in an unbounded fluid comes from a point-force approximation of the spheres, whereas the higher-order terms come from expanding the fundamental solution, in a series of multipoles, to satisfy the no-slip boundary condition at sphere surfaces.

Also using multipole expansions, Sangani & Acrivos (1982) extended Hasimoto's solutions to much larger solid volume fractions. The results of their calculations are given in the form of a series expansion in the solid volume fraction, the coefficients of which are given in table 1 of their paper. Using a boundary-integral method,

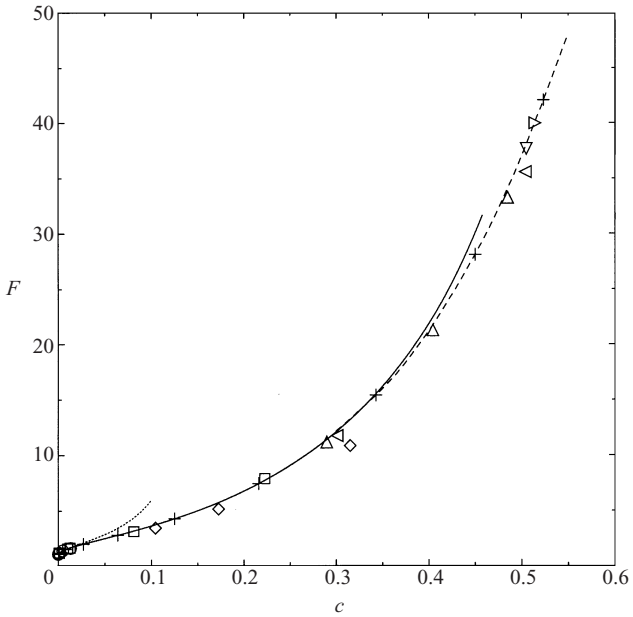

FIGURE 1. The non-dimensional Stokes-flow drag force on the spheres in simple cubic arrays as a function of the solid volume fraction. The symbols are from lattice-Boltzmann simulations with $a = 0.734$ (○), 1.88 (□), 3.8 (◇), 7.8 (△), 15.8 (◁), 16.8 (▽) and 33.8 (▷) lattice units; +, the boundary-integral computations of Zick & Homsy (1982), the dotted line is the $O(c^2)$ theory (9) of Hasimoto (1959), and the solid line is the theory of Sangani & Acrivos (1982). The dashed line interpolates the results of Zick and Homsy.

Zick & Homsy (1982) calculated the drag force on the spheres in ordered arrays at solid volume fractions up to their respective close-packed limits. The error in their computations for close-packed face-centred cubic arrays was estimated to be less than 2%, and hence their results are used in this work as the benchmark with which to compare the results of our lattice-Boltzmann simulations at largest solid volume fractions.

Figure 1 compares the non-dimensional drag force on the spheres in simple cubic arrays calculated from lattice-Boltzmann simulations with the theories of Hasimoto, and Sangani & Acrivos, and with the computations of Zick & Homsy. The effective hydrodynamic radii of the spheres used for these simulations are in the range 0.734–32.8 lattice units, depending on the solid volume fraction. Although it cannot be seen in this figure, the point-force representation of the spheres accurately predicts F at solid volume fractions up to approximately 0.02. The simulations and theory are in excellent agreement at small solid volume fractions, which is to be expected, since the effective hydrodynamic radii of the spheres were calculated using the theory at very small solid volume fractions (see § 2). However, the lattice-Boltzmann simulations are in good agreement with the computations of Zick & Homsy at solid volume fractions up to the close-packed limit, which for simple cubic arrays of spheres is $\pi/6 \approx 0.524$. This comparison demonstrates that the effective hydrodynamic radius obtained from simulations with relatively small nominal radii and small solid volume fractions can be extrapolated to large nominal sphere radii and large solid volume fractions. Consequently, relatively small sphere radii can be used to accurately calculate the Stokes-flow drag force at solid volume fractions much larger than those used to

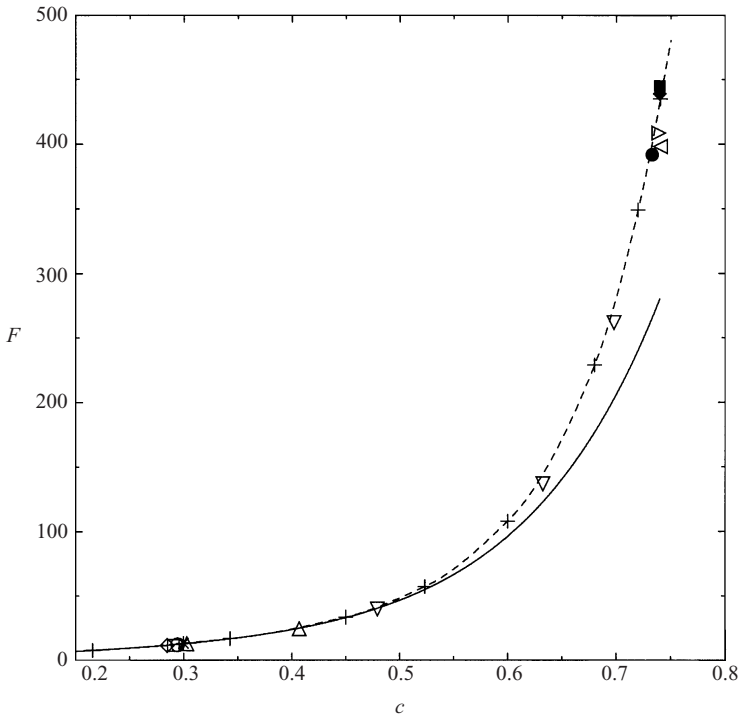

FIGURE 2. The non-dimensional Stokes-flow drag force on the spheres in face-centred cubic arrays as a function of the solid volume fraction. The open symbols are from our lattice-Boltzmann simulations with $a = 7.8$ (○), 8.8 (□), 10.8 (◇), 16.8 (△), 19.8 (◁), 20.8 (▽) and 31.8 (▷) lattice units, and the filled symbols are from the lattice-Boltzmann simulations of Maier *et al.* (1998) with $a = 11.5$ (●), 45.5 (■) and 181 (◆) lattice units; +, the boundary-integral computations of Zick & Homsy (1982), the solid line is the theory of Sangani & Acrivos (1982), and the dashed line interpolates the results of Zick & Homsy.

calculate the effective hydrodynamic radii. For example, an effective hydrodynamic radius of only 1.88 lattice units can be used to accurately calculate F at solid volume fractions up to approximately 0.2.

The number of lattice nodes in the gaps between the spheres decreases with increasing solid volume fraction, and hence larger sphere radii are required to accurately resolve flows at large solid volume fractions. Minimizing the sphere radius is very useful computationally, because the time required for the velocity to reach steady state is proportional to a^2, and the number of lattice nodes is proportional to a^3. It follows that, with a fixed solid volume fraction, the computational cost of the simulations is proportional to a^5. Note that the temporal evolution of these simulations is examined quantitatively in § 5.

Figure 2 compares the non-dimensional Stokes-flow drag force on the spheres in face-centred cubic arrays, calculated from lattice-Boltzmann simulations, with the theory of Sangani & Acrivos and the computations of Zick & Homsy. Also shown are the results of lattice-Boltzmann simulations by Maier *et al.* (1998). At the largest solid volume fractions, these results provide a more rigorous test of the ability of the lattice-Boltzmann method to resolve velocity gradients close to the spheres, since the volume fraction of close-packed face-centred cubic arrays of spheres is $\pi/(3\sqrt{2}) \approx 0.740$, which is considerably larger than the close-packed solid volume fraction of random

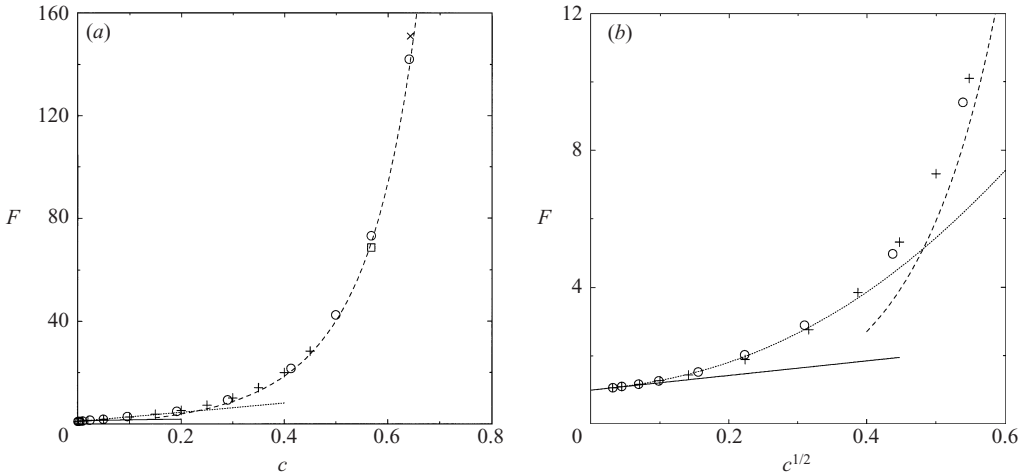

FIGURE 3. (*a*) The non-dimensional Stokes-flow drag force on the spheres in random arrays as a function of the solid volume fraction: ○, lattice-Boltzmann simulations whose parameters and statistical errors are listed in table 1; +, the multipole simulations of Ladd (1990); □, a lattice-Boltzmann simulation of Stokes flow in a cylindrical packed bed of spheres by Maier *et al.* (1998); ×, the experiments of Fand *et al.* (1987). The solid line is the $O(c^{1/2})$ theory of Brinkman 1947, the dotted line is Brinkman's theory with corrections up to $O(c)$ (10) (Kim & Russel 1985), and the dashed line is the Carman correlation (11) (Carman 1937). (*b*) As (*a*) but with the axes scaled to detail the limit of vanishing solid volume fraction.

arrays of spheres, approximately 0.64. As for simple cubic arrays of spheres, moderate sphere radii can be used to accurately calculate the drag force at the largest solid volume fractions.

4.2. *The drag force for random arrays*

Brinkman (1947) calculated the average drag force on the spheres in dilute random arrays by considering a single sphere in an unbounded effective medium whose permeability is determined self-consistently. By including the hydrodynamic interactions between pairs of finite-sized spheres in the effective medium, $O(c \ln c)$ and $O(c)$ corrections to Brinkman's $O(c^{1/2})$ theory have been obtained (Childress 1972; Howells 1974; Hinch 1977). The closed-form expression given by Kim & Russel (1985) is

$$F = 1 + (3/\sqrt{2})c^{1/2} + (135/64)c \ln c + 16.456c + O(c^{3/2}). \tag{10}$$

At larger solid volume fractions, the Carman correlation (Carman 1937), which can be expressed in the form

$$F = 10c/(1-c)^3, \tag{11}$$

gives the average drag force on the spheres in randomly packed beds at solid volume fractions up to the close-packed limit.

Multipole simulations by Ladd (1990), at solid volume fractions up to 0.45, confirm the accuracy of theories for dilute arrays, and show that the Carman correlation can be extrapolated to solid volume fractions considerably smaller than the close-packed limit. More recently, Maier *et at*. (1998) used a lattice-Boltzmann method to simulate Stokes flows in cylindrical packed beds of spheres with much larger solid volume fractions of approximately 0.57. Despite the structure imposed by the walls of the container on the radial distribution of the solid volume fraction, the average Stokes-flow drag force was found to be close to that given by (11).

c	a	L	n_s	n_c	F	$\Delta F/F$
1.04×10^{-3}	0.734	40	40	20	1.089	0.05
1.04×10^{-3}	0.734	80	320	2	1.068	0.03
2.02×10^{-3}	0.734	32	40	20	1.122	0.006
2.02×10^{-3}	0.734	64	320	10	1.109	0.004
4.79×10^{-3}	0.734	24	40	20	1.196	0.009
4.79×10^{-3}	0.734	48	320	10	1.175	0.003
4.79×10^{-3}	0.734	96	2560	2	1.170	0.004
9.66×10^{-3}	0.734	19	40	20	1.289	0.01
9.66×10^{-3}	0.734	38	320	10	1.271	0.003
9.66×10^{-3}	0.734	76	2560	2	1.266	0.007
2.41×10^{-2}	0.734	14	40	10	1.546	0.01
2.41×10^{-2}	0.734	28	320	10	1.529	0.004
4.98×10^{-2}	0.734	11	40	20	2.027	0.02
4.98×10^{-2}	0.734	22	320	10	1.965	0.005
4.98×10^{-2}	0.734	44	2560	2	1.947	8×10^{-5}
9.60×10^{-2}	6.8	76	32	2	2.87	0.004
0.192	8.8	62	16	4	4.98	0.03
0.201	8.8	61	16	5	5.74	0.03
0.290	8.8	54	16	5	9.35	0.03
0.413	8.8	48	16	5	21.5	0.03
0.474	16.8	136	60	1	33.7	—
0.500	16.8	86	16	5	42.0	0.04
0.536	19.8	99	16	1	48.1	—
0.555	17.8	88	16	2	63.1	0.03
0.568	16.8	128	60	1	73.2	—
0.596	20.8	156	60	1	84.6	—
0.633	20.8	124	32	5	129	0.007
0.641	20.8	98	16	2	141	0.06

TABLE 1. Parameters used for lattice-Boltzmann simulations of Stokes flows in random arrays of spheres. The average non-dimensional drag force on the spheres is plotted as a function of the solid volume fraction in figure 3. ΔF is the standard error in the mean of F.

Figure 3 shows the non-dimensional drag force on the spheres in random arrays at solid volume fractions up to the close-packed limit. Figure 3(*b*) shows the same data as in (*a*), but with the axes scaled to detail the limit of vanishing solid volume fraction. The sphere radii and the number of spheres used for each of the simulations are listed in table 1. In many cases, reasonable statistical accuracy could be achieved with as few as 16 spheres in the computational domain, and by ensemble averaging the results from only five random configurations. The standard errors in F, which are typically much less than 5% of the mean, are also listed in table 1.

Our lattice-Boltzmann simulations and the multipole simulations of Ladd both depart from the $O(c)$ theory at a solid volume fraction of approximately 0.2, showing that interactions among more than two spheres in an effective medium become import-

ant at larger solid volume fractions. The Carman correlation is in good agreement with the simulations at solid volume fractions down to approximately 0.3, and, hence, in this range of solid volume fractions, a reasonable 'picture' of the flow is one in which the fluid flows through the tortuous paths in the spaces between the spheres, rather than as a continuous fluid disturbed by widely separated spheres.

4.3. *Finite-size effects for dilute random arrays*

There is a small contribution to the drag force on the spheres in dilute random arrays that diminishes with the number of spheres in the computational domain. A similar effect was observed by Ladd (1990) in the results of his multipole simulations, suggesting that this is an artifact coming from the finite size of the computational domain.

As shown in table 1, simulations with solid volume fractions less than 0.05 were performed with 40, 320 and 2560 spheres in the computational domain, and hence exactly the same solid volume fraction was maintained while the length of the cubic computational domain was precisely doubled. Despite the statistical errors, F consistently decreases with increasing n_s. Note that Durlofsky & Brady (1987) found that the constant offset between the conditionally averaged velocity disturbance obtained from their Stokesian dynamics simulations and the solution of Brinkman's equations decayed as n_s^{-1} at a solid volume fraction of 0.01.

For very small solid volume fractions, the small contribution to the non-dimensional drag force coming from the interactions of the spheres with their periodic images can be shown to be (Hill 2001)

$$F = 1 + (3/\sqrt{2})c^{1/2} + 0.667n_s^{-1}, \tag{12}$$

suggesting that the periodic artifact is independent of the solid volume fraction when c and n_s^{-1} are sufficiently small, and, as suggested by Durlofsky & Brady, is inversely proportional to the number of spheres in the computational domain. Equation (12) was obtained by solving the Brinkman equations with point forces at the vertices of a simple cubic lattice embedded in an unbounded Brinkman medium.

To compare (12) with simulations, equations of the form $F = k_1 + k_2 n_s^{-1}$ were fitted to plots of F versus n_s^{-1} obtained from the simulations with solid volume fractions less than 0.05. As expected from the theory, $k_1 = \partial F/\partial(n_s^{-1})$ did not depend in a systematic way on the solid volume fraction. The average value of $\partial F/\partial(n_s^{-1})$ from the simulations was 0.83, with a standard error of 0.06. When considering the relatively large statistical variations in F relative to the variations that come from changes in n_s, the theory and simulations are in reasonable agreement.

4.4. *The conditionally averaged velocity for random arrays*

Brinkman's theory (Brinkman 1947) gives a simple theoretical description of Stokes flows in dilute random arrays of spheres that quantifies the hydrodynamic interactions among the spheres and gives a closed-form expression for the conditionally averaged velocity (Howells 1974). In this section, the conditionally averaged velocity disturbance obtained from lattice-Boltzmann simulations is compared to that given by Brinkman's equations. This serves to verify the accuracy of the velocity field obtained from the lattice-Boltzmann simulations. Note that Brinkman's theory for the average drag force on the spheres in dilute random arrays is accurate only up to $O(c^{1/2})$. Nevertheless, it is interesting to observe how the conditionally averaged velocity behaves at larger solid volume fractions when the permeability obtained from the simulations is used to calculate the conditionally averaged velocity from Brinkman's equations.

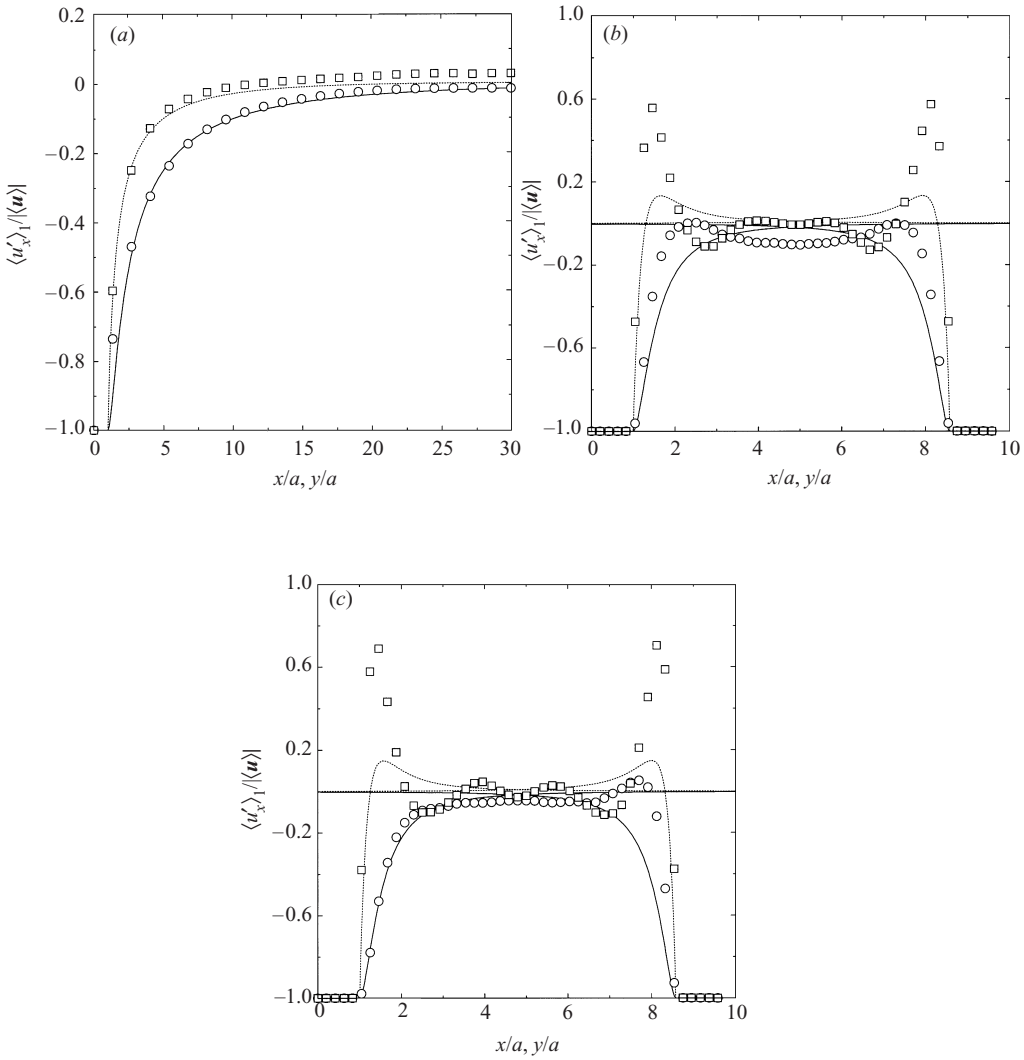

FIGURE 4. The x- (longitudinal) component of the conditionally averaged velocity disturbance as a function of distance from the centre of the test sphere. The symbols are from lattice-Boltzmann simulations of Stokes flows: ○, □ distance in the x- and y- (transverse) directions, respectively. The lines are from the solution of Brinkman's equations (Howells 1974) with the permeability obtained from the simulations. (*a*) $(c, a, n_s, n_c) = (1.04 \times 10^{-3}, 0.734, 40, 20)$; (*b*) (0.305, 4.8, 64, 10); (*c*) (0.305, 4.8, 64, 20).

Figure 4(*a*) shows the variation of the x- (longitudinal) component of the conditionally averaged velocity disturbance as a function of the distance along the x- and y- (transverse) directions from the centre of the test sphere. The symbols identify simulation results, and the lines are from Brinkman's theory. At this very small solid volume fraction, the theory and simulations are in good agreement, even at distances very close to the spheres where the velocity gradients are least resolved. Note that only 40 spheres were used in the computational domain, and hence the small difference between the simulations and the theory at large distances from the test sphere is due to the finite size of the computational domain, as was also observed by Durlofsky & Brady (1987).

At larger solid volume fractions, the theory deviates substantially from the simulations. Figures 4(*a*) and 4(*b*) show conditionally averaged velocity disturbances for Stokes flow and a finite-Reynolds-number flow, respectively, both with a solid volume fraction of 0.305. The most obvious qualitative difference between the theory and simulations occurs in the transverse direction, where, close to the spheres, the velocity is much faster than predicted by the theory. This is also the case in the longitudinal direction, but the velocity does not exceed the average. The faster velocity close to the spheres comes from the excluded volume within two sphere radii of their centres. The variations in the velocity disturbance with radial position come from the finite size of the computational domain and the non-uniform pair probability that gives a non-uniform permeability. However, at the furthest distance from the test sphere – halfway between the test sphere and its periodic image – the conditionally averaged velocity is within 5% of the average velocity.

As shown in figure 4(*c*), the effect of fluid inertia at a Reynolds number of approximately 9 is to break the symmetry of the Stokes flow about the plane passing through the centre of the test sphere and whose unit normal is parallel to the x-axis. The broken symmetry results in faster moving fluid close to the spheres on their upstream side and slower moving fluid close to the spheres on their downstream side. The slightly larger variations in the velocity disturbance relative to Stokes flow shows that more fluid flows through regions where the permeability is relatively high. Such regions occur very close to the spheres – in the excluded volume region – and at distances far from the spheres where the conditionally averaged velocity has local maxima.

5. Unsteady flows with zero Reynolds number

In this section, the evolution of the average velocity and drag force on the spheres in fixed arrays is examined when the fluid is accelerated from rest, by a constant body force, toward a steady-Stokes-flow. Theoretical and computational predictions of the steady-Stokes-flow velocity variance are used to compute the long-time added mass coefficient and, hence, the long-time relaxation of the average fluid velocity to its steady-state value.

An equation for the temporal evolution of the average velocity can be obtained by equating the time rate of change of the average fluid momentum to the forces exerted on the fluid by the average pressure gradient and the spheres. Using (5) to express the force on the spheres in terms of a time-dependent non-dimensional force, F, and the average pressure gradient in terms of the steady-state non-dimensional drag force, F_∞, gives

$$\rho \mathrm{d}|\langle \boldsymbol{u} \rangle|/\mathrm{d}t = n6\pi\mu a(F_\infty|\langle \boldsymbol{u} \rangle|_\infty - F|\langle \boldsymbol{u} \rangle|). \tag{13}$$

The time-dependent force on each sphere can be expressed in the form (Sangani, Zhang & Prosperetti 1991)

$$\boldsymbol{f} = F6\pi\mu a\langle \boldsymbol{u} \rangle = (1 + C_a/2)\rho(4/3)\pi a^3 \mathrm{d}\langle \boldsymbol{u} \rangle/\mathrm{d}t + F_\infty 6\pi\mu a\langle \boldsymbol{u} \rangle + \boldsymbol{f}_h, \tag{14}$$

where C_a is the added-mass coefficient and $\boldsymbol{f}_h$ is the Basset history force. The factor of $(1 + C_a/2)$ in the first term on the right-hand side of (14) comes from the acceleration of the fluid relative to the spheres, which contributes the factor $C_a/2$, and from the acceleration of the fluid relative to a fixed frame of reference, which contributes the factor of one. The latter comes from the constant pressure gradient required to accelerate the fluid (Batchelor 1967). At short and long times, the Basset history

force, which comes from the transient diffusion of vorticity throughout the fluid, can be neglected, since in these limits the force on the spheres is dominated by the contributions from the quasi-steady drag and added-mass forces.

Substituting (14) into (13) and neglecting the Basset history force gives

$$|\langle \boldsymbol{u} \rangle| = |\langle \boldsymbol{u} \rangle|_\infty [1 - \exp(-t/\tau)], \tag{15}$$

where

$$\tau v/a^2 = 2/(9cF_\infty) + (2 + C_a)/(9F_\infty). \tag{16}$$

Hence, provided that the Basset history force can be neglected, the average velocity relaxes exponentially toward steady state with a relaxation time constant τ. The first term on the right-hand side of (16) is simply the time that it would take to accelerate the fluid from rest to the steady-state velocity in the absence of the spheres. The second term is the non-trivial contribution to the relaxation time constant that comes from the transient development of the flow.

The time-dependent non-dimensional force can be obtained by substituting (15) into (14), which gives

$$F/F_\infty = 1 + \frac{c(1 + C_a/2)\exp(-t/\tau)}{[1 + c(1 + C_a/2)][1 - \exp(-t/\tau)]}, \tag{17}$$

where C_a has yet to be determined.

At short times, the flow outside a boundary layer at the sphere surfaces is inviscid and irrotational, and hence the velocity is similar to that for rapidly oscillating flow. Sangani *et al.* (1991) calculated the added-mass coefficient of the spheres in ordered and random suspensions subjected to a small-amplitude oscillatory flow. They showed that the added-mass coefficient does not depend very much on the relative density of the solid and fluid phases, and hence their results for neutrally buoyant particles with a no-slip boundary condition at their surfaces gives a reasonable approximation for fixed spheres. Their theoretical result for simple cubic arrays is

$$C_a = (1 + 2c)/(1 - c) + O(c^{10/3}), \tag{18}$$

which is in good agreement with their computations over a wide range of solid volume fractions. Furthermore, the added-mass coefficient does not depend very much on the sphere configuration, and hence (18) is a reasonable approximation for random arrays of spheres.

At long times, the flow is viscous and quasi-steady, and the added-mass coefficient can be calculated by equating the time rate of change of the kinetic energy of the fluid, in a frame of reference moving with the average velocity, to the sum of the rate of work done by the drag force on the spheres and the rate of viscous dissipation. Note that the assumption of quasi-steady flow allows the slowly evolving velocity variance to be expressed in terms of the steady-state velocity variance, and hence

$$\langle \boldsymbol{u}' \cdot \boldsymbol{u}' \rangle / |\langle \boldsymbol{u} \rangle|^2 = \langle \boldsymbol{u}' \cdot \boldsymbol{u}' \rangle_\infty / |\langle \boldsymbol{u} \rangle|^2_\infty, \tag{19}$$

where $\boldsymbol{u}' = \boldsymbol{u} - \langle \boldsymbol{u} \rangle$. If it is assumed that the rate of viscous dissipation is to leading order equal to the rate of work done by the quasi-steady drag force, then there remains in the energy conservation equation

$$(\rho/2)\mathrm{d}\langle \boldsymbol{u}' \cdot \boldsymbol{u}' \rangle/\mathrm{d}t = \rho c(1 + C_a/2)\langle \boldsymbol{u} \rangle \cdot \mathrm{d}\langle \boldsymbol{u} \rangle/\mathrm{d}t, \tag{20}$$

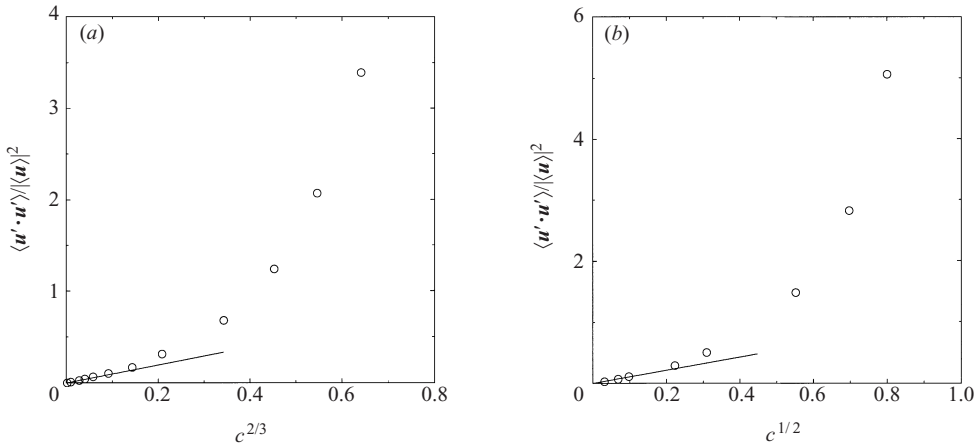

FIGURE 5. (*a*) The velocity variance for steady Stokes flows in simple cubic arrays of spheres as a function of the solid volume fraction. The symbols are from lattice-Boltzmann simulations and the line is the $O(c^{2/3})$ theory (25). (*b*) As (*a*) for steady Stokes flows in random arrays of spheres but the symbols are from lattice-Boltzmann simulations, and the line is the $O(c^{1/2})$ theory (30).

which together with (19) gives

$$C_a/2 = \frac{\langle \boldsymbol{u}' \cdot \boldsymbol{u}' \rangle_\infty}{c|\langle \boldsymbol{u} \rangle|_\infty^2} - 1. \tag{21}$$

For dilute simple cubic arrays of spheres, the steady-state velocity disturbance can be calculated from the fundamental periodic solution of the Stokes equations (Hasimoto 1959). The velocity disturbance is

$$\boldsymbol{u}' = \sum_{\boldsymbol{k} \neq \boldsymbol{0}} \hat{\boldsymbol{u}}' \exp(-2\pi \mathrm{i} \boldsymbol{k} \cdot \boldsymbol{x}), \tag{22}$$

where

$$\hat{\boldsymbol{u}}' = -\frac{\boldsymbol{f} \cdot (\boldsymbol{I} - \boldsymbol{k}\boldsymbol{k}/k^2)}{(2\pi k)^2} \tag{23}$$

are the Fourier coefficients of the velocity disturbance, and $\boldsymbol{k}$ is the dimensionless wavenumber vector. The velocity is non-dimensionalized with the magnitude of the average velocity, $|\langle \boldsymbol{u} \rangle|$, distance with the sphere separation, L, and the drag force with $\mu|\langle \boldsymbol{u} \rangle|L$.

The steady-state velocity variance can be calculated from the integral of $\boldsymbol{u}' \cdot \boldsymbol{u}'$ over the volume of a cubic unit-cell. This integral can be simplified to a single sum in Fourier space,

$$\langle \boldsymbol{u}' \cdot \boldsymbol{u}' \rangle = \sum_{\boldsymbol{k} \neq \boldsymbol{0}} \hat{\boldsymbol{u}}' \cdot \hat{\boldsymbol{u}}'. \tag{24}$$

Evaluating the sum in (24), and using the approximation that $F \sim 1$, gives

$$\langle \boldsymbol{u}' \cdot \boldsymbol{u}' \rangle / |\langle \boldsymbol{u} \rangle|^2 = 0.9669 c^{2/3} + O(c). \tag{25}$$

Figure 5(*a*) shows the steady-state velocity variance for simple cubic arrays of spheres as a function of the solid volume fraction. The theory (25) and the simulations are in excellent agreement at the very small solid volume fractions where the point-force

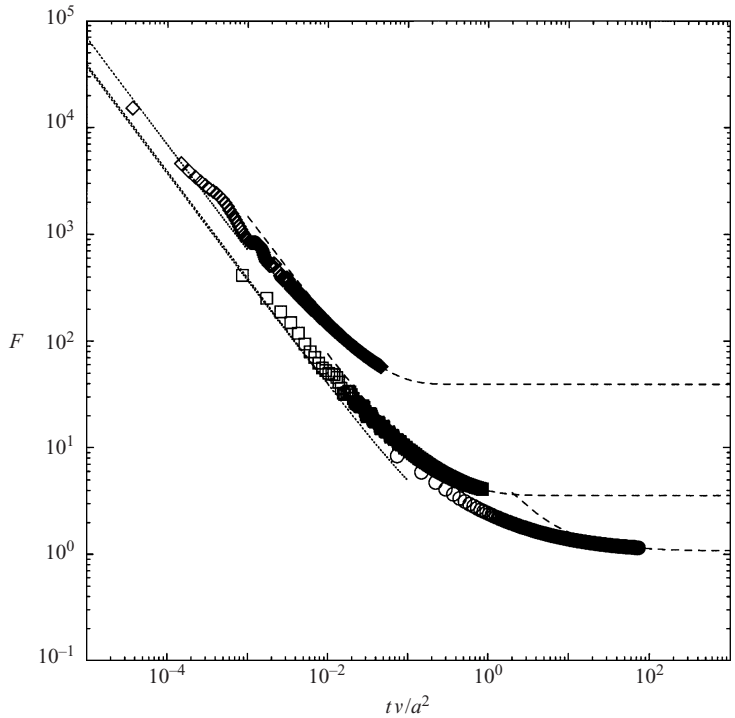

FIGURE 6. The time series of the non-dimensional drag force on the spheres in simple cubic arrays when the fluid is accelerated from rest by a constant average pressure gradient toward a steady Stokes flow. The symbols are from lattice-Boltzmann simulations with $(c, a) = 1.06 \times 10^{-4}, 0.734)$ (○), (0.0953, 6.8) (□), and (0.514, 32.8) (◇), where a is lattice units. The dotted and dashed lines are the theory (17) for the limits $t \to 0$ and $t \to \infty$, respectively.

representation of the spheres accurately predicts F, i.e. when Hasimoto's $O(c^{1/3})$ theory (9) is accurate.

For dilute random arrays of spheres, the steady-state velocity variance can be calculated from the conditionally averaged velocity disturbance, which can be approximated by the fundamental solution of the Brinkman equations,

$$\nabla\langle p\rangle_1 + \langle \boldsymbol{u}\rangle_1 - \nabla^2\langle \boldsymbol{u}\rangle_1 + \delta(\boldsymbol{x})\langle \boldsymbol{f}\rangle_1 = 0 \quad \text{and} \quad \nabla\cdot\langle \boldsymbol{u}\rangle_1 = 0, \tag{26}$$

where the velocity is non-dimensionalized with the magnitude of the average velocity, $|\langle \boldsymbol{u}\rangle|$, distance with the Brinkman screening length, ℓ, pressure with $\mu|\langle \boldsymbol{u}\rangle|/\ell$, and the drag force with $\mu|\langle \boldsymbol{u}\rangle|\ell$.

From the Fourier transform of (26), the conditionally averaged velocity disturbance is

$$\langle \boldsymbol{u}'\rangle_1 = \int \langle \hat{\boldsymbol{u}}'\rangle_1 \exp(-2\pi \mathrm{i}\boldsymbol{k}\cdot\boldsymbol{x})\, \mathrm{d}\boldsymbol{k}, \tag{27}$$

where the Fourier coefficients of the velocity disturbance are

$$\langle \hat{\boldsymbol{u}}'\rangle_1 = -\frac{\langle \boldsymbol{f}\rangle_1\cdot(\boldsymbol{I} - \boldsymbol{k}\boldsymbol{k}/k^2)}{1 + (2\pi k)^2}, \tag{28}$$

and $\boldsymbol{k}$ is the dimensionless wavenumber vector.

In the limit of vanishing solid volume fraction, the steady-state velocity variance can be calculated from the integral of $n\langle \boldsymbol{u}'\rangle_1\cdot\langle \boldsymbol{u}'\rangle_1$ over all positions of the test sphere

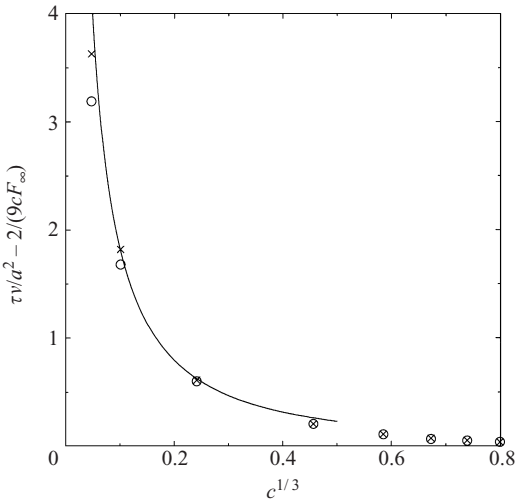

FIGURE 7. The contribution of the added-mass and quasi-steady drag forces on the spheres in simple cubic arrays to the relaxation time constant at long times as a function of the solid volume fraction: ×, obtained by fitting an exponential function (15) to time series of the average velocity obtained from simulations; ○, the circles are the theory (16) with the steady-state velocity variance and non-dimensional drag force obtained from simulations, and the line is the theory with the steady-state velocity variance and nondimensional drag force calculated from (25) and the $O(c^{1/3})$ theory of Hasimoto (1959) (9), respectively.

(Koch & Brady 1985). This integral can be simplified to a single integral in Fourier space,

$$\langle \boldsymbol{u}' \cdot \boldsymbol{u}' \rangle = n \int \langle \hat{\boldsymbol{u}}' \rangle_1 \cdot \langle \hat{\boldsymbol{u}}' \rangle_1 \, \mathrm{d}\boldsymbol{k}, \tag{29}$$

which can be evaluated to give

$$\langle \boldsymbol{u}' \cdot \boldsymbol{u}' \rangle / |\langle \boldsymbol{u} \rangle|^2 = 3c^{1/2}/(2\sqrt{2}) + O(c), \tag{30}$$

where, as for simple cubic arrays, only the leading-order approximation for F has been used, since the point-force representation of the test sphere gives the velocity variance only up to $O(c^{1/2})$.

Figure 5(*b*) shows the steady-state velocity variance for random arrays of spheres as a function of the solid volume fraction. As for simple cubic arrays, the theory (30) and the simulations are in excellent agreement at the very small solid volume fractions where the point-force representation of the spheres accurately predicts F, i.e. when Brinkman's $O(c^{1/2})$ theory (10) is accurate (see figure 4).

Having now determined the steady-state velocity variance for simple cubic and random arrays of spheres and, hence, the long-time added-mass coefficient, the relaxation time constant, which depends on c, F_∞ and C_a, can be compared to simulation results. First, the temporal evolution of F given by the theory for short and long times is compared to the time series obtained from simulations.

Figure 6 compares the theoretical predictions for the short- and long-time evolution of the non-dimensional drag force on the spheres in simple cubic arrays with time series obtained from simulations with representative solid volume fractions of 1.06×10^{-4}, 0.0953 and 0.514. Note that, at a solid volume fraction of 1.06×10^{-4}, the steady-state velocity variance and non-dimensional drag force were calculated from (25) and the $O(c^{1/3})$ theory of Hasimoto (9), respectively, whereas at the larger solid volume

fractions they were obtained from the simulations. The simulations and theory are in good agreement at short and long times and over the entire range of solid volume fractions. This not only confirms the accuracy of the lattice-Boltzmann method for time-dependent problems, but shows that the Basset history force can be neglected at short and long times. It also justifies the assumptions of potential flow at short times and quasi-steady viscous flow at long times.

Figure 7 shows the contribution of the added-mass and quasi-steady forces to the relaxation time constant at long times as a function of the solid volume fraction. At very small solid volume fractions, the steady-state velocity variance and non-dimensional drag force were calculated from (25) and (9), respectively (circles). Also shown is the theory with the steady-state velocity variance and non-dimensional drag force obtained from the simulations (line). These are in good agreement with the relaxation time constant obtained by fitting an exponential function to the time series from simulations (crosses). Note that, in the limit of vanishing solid volume fraction, the contribution of the added-mass force to the relaxation time constant is $O(c^{-1/3})$. This scaling can be deduced by balancing the $O(cC_a|\langle \boldsymbol{u}\rangle|\mathrm{d}|\langle \boldsymbol{u}\rangle|/\mathrm{d}t)$ rate of work done by the added-mass force with the $O(c^{2/3}\mathrm{d}|\langle \boldsymbol{u}\rangle|^2/\mathrm{d}t)$ rate at which the kinetic energy of the fluid increases.

Note that the temporal evolution of the average velocity in random arrays of spheres can also be accurately predicted by this theory. For example, with $(c, a, n_s) = (0.641, 20.8,\ 16)$, lattice-Boltzmann simulations give $\langle \boldsymbol{u}' \cdot \boldsymbol{u}' \rangle = 5.06|\langle \boldsymbol{u}\rangle|^2$ and $F_\infty = 134.6$. Therefore, from equations (21) and (16), $C_a/2 = 6.89$ and $\tau v/a^2 = 0.0156$, respectively. The latter is in good agreement with $\tau v/a^2 = 0.0155$ obtained from the time series of the average velocity. Figure 8 compares the temporal evolution of F from the simulations with the theory. The potential-flow approximation breaks down relatively quickly, because the vorticity generated at the sphere surfaces rapidly fills the small gaps between the spheres. However, this is also the reason why the quasi-steady viscous-flow approximation is successful at longer times.

6. Steady flows with small but finite Reynolds numbers

Now that the lattice-Boltzmann method has been validated for steady and unsteady flows when the Reynolds number is zero, the first effects of fluid inertia on steady flows in ordered and random arrays may be examined. In this section, theories are compared to the results of simulations, showing the ranges of the Reynolds number and solid volume fraction over which they are accurate.

6.1. *Theory for dilute ordered arrays*

The theory developed here gives the dependence of the drag force on the spheres in dilute simple cubic arrays on the Reynolds number and the solid volume fraction when $Re \ll 1$. The spheres are represented by point forces, $-\delta(\boldsymbol{x})\boldsymbol{f}$, acting on the fluid, and hence the solid volume fraction is required to be small. Simulations are compared to the theory to show the range of solid volume fractions over which the point-force representation is accurate.

For convenience, only a single sphere in a unit-cell with periodic boundary conditions needs to be considered. At distances far from the spheres, the Navier–Stokes equations can be approximated by the Oseen equations,

$$Re_L\langle \boldsymbol{u}\rangle \cdot \nabla \boldsymbol{u} + \nabla p - \nabla^2 \boldsymbol{u} + \delta(\boldsymbol{x})\boldsymbol{f} = 0 \quad \text{and} \quad \nabla \cdot \boldsymbol{u} = 0, \tag{31}$$

where the velocity is non-dimensionalized with the magnitude of the average velocity,

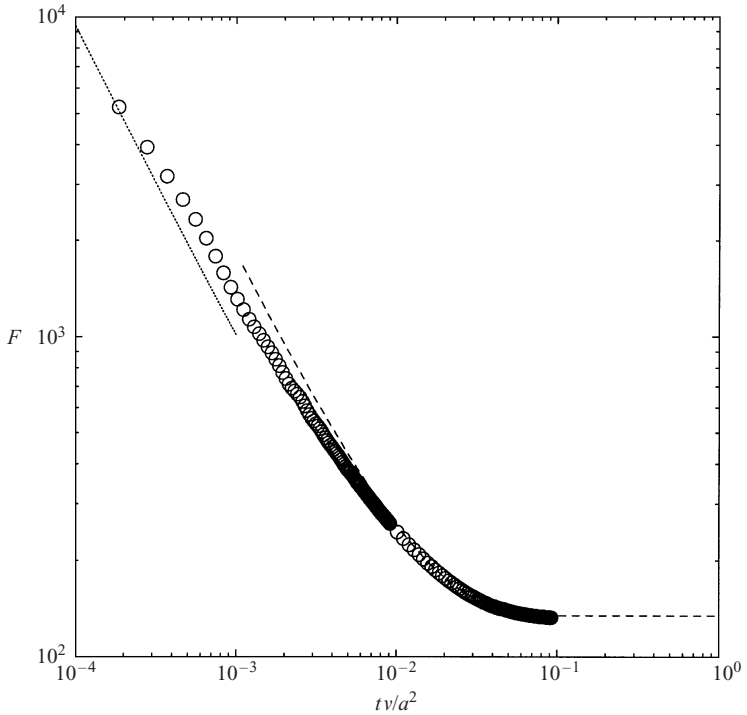

FIGURE 8. The time series of the average non-dimensional drag force on the spheres in a close-packed random array of spheres when the fluid is accelerated from rest, by a constant average pressure gradient, toward a steady Stokes flow. The symbols are from a lattice-Boltzmann simulation with $(c, a, n_s) = (0.641, 20.8, 16)$, where a is in lattice units. The dotted and dashed lines are the theory (17) for the limits $t \to 0$ and $t \to \infty$, respectively. The short-time added mass coefficient was obtained from the theory of Sangani *et al.* (1991) (18), and the steady-state velocity variance used to calculate the long-time added-mass coefficient was obtained from the simulation.

$|\langle \boldsymbol{u} \rangle|$, distance with the sphere separation, L, pressure with $\mu|\langle \boldsymbol{u} \rangle|/L$, and the drag force with $\mu|\langle \boldsymbol{u} \rangle|L$.

From the discrete Fourier transform of (31), the Fourier coefficients of the fluid velocity disturbance in this outer region are

$$\hat{\boldsymbol{u}}' = -\frac{\boldsymbol{f} \cdot (\boldsymbol{I} - \boldsymbol{k}\boldsymbol{k}/k^2)}{2\pi \mathrm{i} Re_L \langle \boldsymbol{u} \rangle \cdot \boldsymbol{k} + (2\pi k)^2}, \tag{32}$$

where $\boldsymbol{k}$ is the dimensionless wavenumber vector. The velocity can be conveniently written in the form

$$\boldsymbol{u} = \langle \boldsymbol{u} \rangle + \boldsymbol{u}_s + \boldsymbol{u}_o, \tag{33}$$

where from (32)

$$\boldsymbol{u}_s = -\sum_{\boldsymbol{k} \neq \boldsymbol{0}} \frac{\boldsymbol{f} \cdot (\boldsymbol{I} - \boldsymbol{k}\boldsymbol{k}/k^2)}{(2\pi k)^2} \exp(-2\pi \mathrm{i} \boldsymbol{k} \cdot \boldsymbol{x}) \tag{34}$$

and

$$\boldsymbol{u}_o = \sum_{\boldsymbol{k} \neq \boldsymbol{0}} \frac{\boldsymbol{f} \cdot (\boldsymbol{I} - \boldsymbol{k}\boldsymbol{k}/k^2)(2\pi Re_L \langle \boldsymbol{u} \rangle \cdot \boldsymbol{k})^2}{(2\pi k)^6 + (2\pi)^2 (2\pi Re_L \langle \boldsymbol{u} \rangle \cdot \boldsymbol{k})^2} \exp(-2\pi \mathrm{i} \boldsymbol{k} \cdot \boldsymbol{x}). \tag{35}$$

These are the Stokes-flow and inertial (Oseen) disturbances to the average fluid velocity, respectively.

To match this outer solution to the inner Stokes flow, the terms on the right-hand side of (33) need to be evaluated only in the limit $x \to 0$. The inertial velocity disturbance can be obtained by evaluating the sum in (35) directly, since in the limit $x \to 0$ it is independent of position.

Note that, in the limits $Re_L \to \infty$ and $x \to 0$, the sum in (35) can be approximated by an integral, which can be evaluated exactly to give

$$\boldsymbol{u}_o = \boldsymbol{f} Re_L/(16\pi). \tag{36}$$

This leads to Oseen's result for the first inertial contribution to the Stokes-flow drag force on a single sphere in an unbounded fluid (Batchelor 1967),

$$F = 1 + (3/8)Re. \tag{37}$$

In the limit $Re_L \to 0$, (35) becomes

$$\boldsymbol{u}_o = Re_L^2 \sum_{\boldsymbol{k}\neq\boldsymbol{0}} \frac{\boldsymbol{f}\cdot(\boldsymbol{I}-\boldsymbol{k}\boldsymbol{k}/k^2)(\langle\boldsymbol{u}\rangle\cdot\boldsymbol{k})^2}{(2\pi)^4 k^6} \exp(-2\pi \mathrm{i}\boldsymbol{k}\cdot\boldsymbol{x}) + O(Re_L^4), \tag{38}$$

which, in the limit $x \to 0$, becomes

$$u_{oi} = Re_L^2/(2\pi)^4 \left(4.75 f_i - 1.53 f_j \langle u\rangle_i \langle u\rangle_j - 1.69 \delta_{ijkl} f_j \langle u\rangle_k \langle u\rangle_l\right), \tag{39}$$

where summation over repeated indices is implied. Note that $\delta_{ijkl} = 1$ when $i = j = k = l$, otherwise $\delta_{ijkl} = 0$. When $\langle\boldsymbol{u}\rangle$ is directed along the x-axis, (39) simplifies to

$$\boldsymbol{u}_o = 1.53 Re_L^2 \boldsymbol{f}/(2\pi)^4. \tag{40}$$

The outer Stokes-flow velocity disturbance was first calculated by Hasimoto 1959. In the limit $x \to 0$, it is

$$\boldsymbol{u}_s = 8\pi \boldsymbol{f}\cdot\left(2.8373(4/3)\boldsymbol{I} - \boldsymbol{I}/x - \boldsymbol{x}\boldsymbol{x}/x^3\right) + O(x^{-2}). \tag{41}$$

The velocity in the inner region can be approximated by that for Stokes flow past a finite-sized sphere in an unbounded fluid with a constant velocity $\langle\boldsymbol{u}\rangle_\infty$ far from the sphere (Batchelor 1967). After non-dimensionalizing the velocity and distance with $|\langle\boldsymbol{u}\rangle|$ and L, respectively, the velocity in the inner region, as $x \to \infty$, is

$$\boldsymbol{u} = \langle\boldsymbol{u}\rangle_\infty \cdot \left(\boldsymbol{I} - 3a/(4L)\boldsymbol{I}/x - 3a/(4L)\boldsymbol{x}\boldsymbol{x}/x^3\right) + O(x^{-2}). \tag{42}$$

Matching the terms in (42) and (39) that decay as x^{-1}, as well as those that are independent of position, leads to

$$F = 1 + 1.7601 c^{1/3} + 0.030 c^{-1/3} Re^2 + O(Re_L^4). \tag{43}$$

Simulations of flows in dilute simple cubic arrays of spheres were performed with Reynolds numbers such that $Re_L = O(c^{-1/3}Re) \ll 1$. As expected from the theory, F increased linearly with Re^2, and hence, by plotting F versus Re^2, the coefficients F_0 and F_1 in equations of the form

$$F = F_0 + F_1 Re^2 \tag{44}$$

were obtained at various solid volume fractions. From the theory, $F_1 = 0.030 c^{-1/3}$, which, as shown in figure 9, is consistent with the simulations. However, there are $O(1)$ and $O(c^{1/3})$ corrections to the theory that can be obtained from the simulations. These scalings can be deduced by considering reflections of the $O(a/L) = O(c^{1/3})$

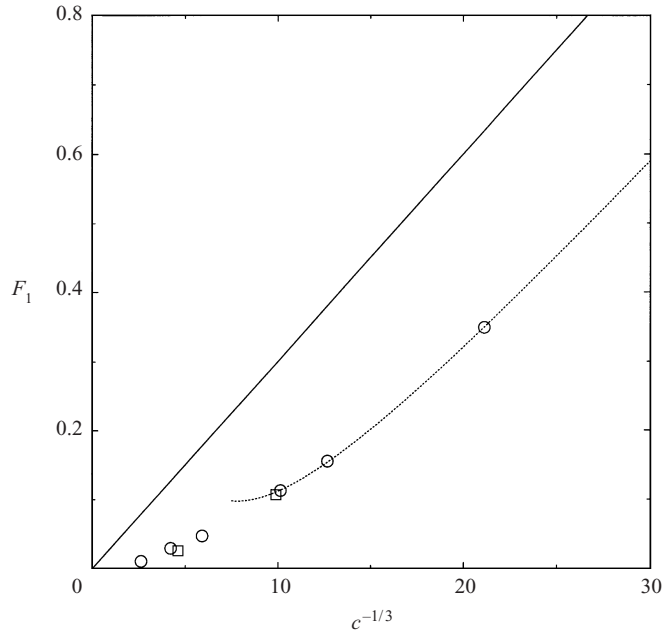

FIGURE 9. The coefficient of the $O(Re^2)$ inertial contribution to the non-dimensional drag force on the spheres in dilute simple cubic arrays. The symbols are from simulations with $a = 0.734$ (○) and 1.88 (□) lattice units. The solid line is the $O(c^{-1/3})$ theory (43) based on the Oseen approximation, and the dotted line is the theory (45) with the $O(1)$ and $O(c^{1/3})$ corrections that were obtained from the simulations.

velocity disturbance produced by each sphere at its nearest neighbours. Fitting an equation of the form $F_1 = 0.030c^{-1/3} + k_1 + k_2c^{1/3}$ to the simulation results gives $k_1 = -0.37$ and $k_2 = 1.8$, and hence

$$F = 1 + 1.7601c^{1/3} + (0.030c^{-1/3} - 0.37 + 1.8c^{1/3})Re^2, \tag{45}$$

which, as shown in figure 9, fits the simulation results at solid volume fractions up to approximately 10^{-3}.

Figure 10 shows the inertial contribution to the non-dimensional drag force on the spheres in a simple cubic array with a solid volume fraction of 9.59×10^{-4} as a function of the angle between the average pressure gradient and the x-axis in the (x, y)-plane, θ_p. Note that the $O(1)$ and $O(c^{1/3})$ corrections to F that were obtained from the simulations when $\theta_p = 0$ have been added to the theory for all θ_p. The excellent agreement between the simulations and theory shows that the dependence of the drag force on the direction of the flow is captured entirely at $O(c^{-1/3})$.

Figure 11 shows the theory (solid line) for all values of Re_L when the average velocity is directed along the x-axis. Also shown are results from simulations with a solid volume fraction of 9.59×10^{-4} (circles). The large difference between the simulations and theory when Re_L is large comes from the breakdown of the Oseen approximation, which is accurate for a single sphere in an unbounded fluid only when $Re < 0.005$. The dot-dashed line in figure 11 was obtained by subtracting from the theory the difference between the non-dimensional drag force on a single sphere in an unbounded fluid given by Oseen's equation (37) and that given by the empirical

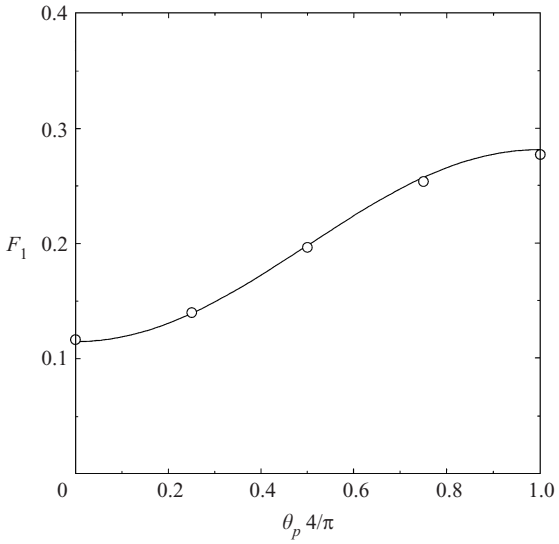

FIGURE 10. The coefficient of the $O(Re^2)$ inertial contribution to the non-dimensional drag force on the spheres in a simple cubic array with $c = 9.59 \times 10^{-4}$ as a function of the angle between the average pressure gradient and the x-axis in the (x, y)-plane. The symbols are from simulations with $a = 0.734$ lattice units, and the line is the theory with an inertial velocity disturbance given by (39). The $O(1)$ and $O(c^{1/3})$ corrections to the $O(c^{-1/3})$ theory for $\theta_p = 0$ have been added to the theory for all θ_p.

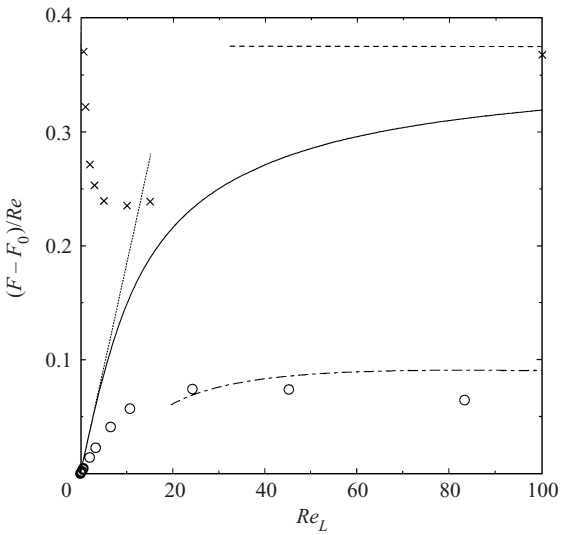

FIGURE 11. The first inertial contribution to the non-dimensional drag force on the spheres in dilute simple cubic arrays, divided by the Reynolds number based on the sphere radius, as a function of the Reynolds number based on the sphere separation when the average pressure gradient is directed along the x-axis. The solid line is the theory for all Re_L, and the dotted and dashed lines are the theory for $Re_L \to 0$ and $Re_L \to \infty$, respectively. ○, lattice-Boltzmann simulations with $(c, a) = (9.59 \times 10^{-4}, 0.734)$, where a is in lattice units, and the dash-dotted line is the theory (solid line) with a correction for the breakdown of the Oseen approximation at finite Reynolds numbers. ×, the theory of Cheng & Papanicolaou (1997).

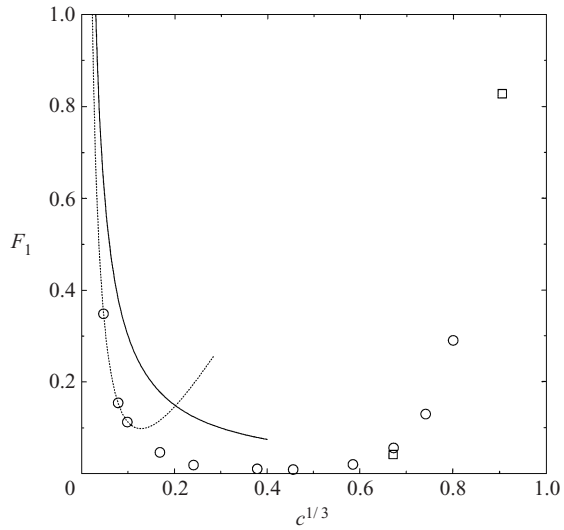

FIGURE 12. The coefficient of the $O(Re^2)$ inertial contribution to the non-dimensional drag force on the spheres in simple cubic (○) and face-centred cubic (□) arrays as a function of the solid volume fraction. The symbols are from lattice-Boltzmann simulations and the solid line is the $O(c^{-1/3})$ theory (45) for simple cubic arrays of spheres. The dotted line is the theory with $O(1)$ and $O(c^{1/3})$ corrections that were obtained from the simulations.

correlations recommended by Clift, Grace & Weber (1978),

$$F = \begin{cases} 1 + (3/8)Re & (Re \leqslant 0.005) \\ 1 + 0.1315(2Re)^{0.82-0.05\log(2Re)} & (0.005 < Re \leqslant 10) \\ 1 + 0.2996Re^{0.6305} & (10 < Re < 130). \end{cases} \tag{46}$$

Although this simple correction for finite Reynolds numbers neglects hydrodynamic interactions, it gives an excellent approximation of the drag force when Re_L is greater than approximately 20. This shows that inertial effects beyond the Oseen approximation are manifested at length scales much smaller than the $O(a/Re)$ Oseen distance. Unfortunately, the long time that it takes for the velocity to reach steady state at such small solid volume fractions makes simulations with smaller solid volume fractions prohibitively expensive.

Cheng & Papanicolaou (1997), whose theory was discussed briefly in the introduction, presented the results of their theory as a table of $\Delta F = (F-1)/Re$ as a function of Re_L. Therefore, the ordinate in figure 11 is $(F - F_0)/Re = \Delta F - \Delta F_0$, where ΔF_0 is actually F_0/Re, which is given by Hasimoto's $O(c^{1/3})$ theory for the Stokes-flow drag force. In the limit $Re_L \to 0$, the ordinate fits an equation of the form $k_1 + k_2/Re_L$ when $Re_L < 0.6$, which gives an inertial contribution to F that is proportional to Re instead of Re^2. Furthermore, although their results approach the correct asymptote in the limit $Re_L \to \infty$, the approach is clearly much more rapid than our theory suggests.

6.2. *Computational results for ordered arrays at moderate solid volume fractions*

Having confirmed that the first inertial contribution to the non-dimensional drag force on the spheres in dilute simple cubic arrays is proportional to Re^2, this scaling is now examined at solid volume fractions up to the close-packed limit. The theory of Mei & Auriault (1991) predicts that this scaling is independent of the solid volume fraction, provided that the Reynolds number is sufficiently small.

Figure 12 shows the coefficient of the $O(Re^2)$ inertial contribution to the non-dimensional drag force on the spheres in simple cubic arrays (circles) at solid volume fractions up to the close-packed limit. The average pressure gradient is directed along the x-axis. With increasing solid volume fraction, the inertial contribution to the drag force first decreases, reaching a minimum at a solid volume fraction of approximately 0.1, and then increases as the solid volume fraction approaches the close-packed limit. Also shown in figure 12 are simulation results for face-centred cubic arrays of spheres (squares) with solid volume fractions of approximately 0.3 and 0.75. These show that the first inertial contribution to F does not depend significantly on the sphere configuration.

Although the inertial contribution to the drag force increases with the solid volume fraction as the solid volume fraction approaches the close-packed limit, it is not easy to measure experimentally. The first effects of fluid inertia actually diminish at large solid volume fractions, because the Stokes-flow drag force, F_0, increases much more rapidly with the solid volume fraction than F_1. This was also the case for the arrays of aligned cylinders examined by Koch & Ladd (1997).

6.3. *Random arrays*

Kaneda (1986) calculated the first inertial contribution to the drag force on the spheres in dilute random arrays. The Brinkman screening length plays a similar role in Kaneda's theory as the sphere separation does in the theory presented above for simple cubic arrays. Although the Reynolds number based on the Brinkman screening length can take any value in Kaneda's theory, only the limit in which $Re_\ell \to 0$ is considered here, because simulations with $Re_\ell \gg 1$ and $Re \ll 1$ are prohibitively expensive. Note, however, that an estimate of the inertial contribution to the drag force in the limit $Re_\ell \to \infty$ could be obtained by correcting Kaneda's theory using the finite-Reynolds-number drag force on a single sphere in an unbounded fluid, as demonstrated above for simple cubic arrays of spheres, and by Koch & Ladd (1997) for random arrays of aligned cylinders.

Simulations of flows in a dilute random array of spheres were performed with Reynolds number such that $Re_\ell \ll 1$. As expected from theory, F increased linearly with Re^2, and hence, by plotting F versus Re^2, the coefficients F_0 and F_1 in equations of the form (44) were obtained at various solid volume fractions. For dilute arrays, Kaneda's theory gives $F_1 = (\sqrt{2}/40)c^{-1/2}$, which, as shown in figure 13, is consistent with the simulations. However, there are $O(1)$ and $O(c^{1/2})$ corrections to Kaneda's theory that can be obtained from the simulations. Fitting an equation of the form $F_1 = \sqrt{2}/40c^{-1/2}+k_1+k_2c^{1/2}$ to the simulation results gives $k_1 = -0.182$ and $k_2 = 1.01$, and hence

$$F_1 = (\sqrt{2}/40)c^{-1/2} - 0.182 + 1.01c^{1/2}, \tag{47}$$

which, as shown in figure 13, fits the simulation results at solid volume fractions up to approximately 0.03.

Figure 14 shows F_1 at solid volume fractions up to the close-packed limit. Similarly to simple cubic arrays of spheres, the inertial contribution to the drag force first decreases with increasing solid volume fraction, reaches a minimum at a solid volume fraction of approximately 0.1, and then increases rapidly as the solid volume fraction approaches the close-packed limit. The results shown here with solid volume fractions greater than approximately 0.1 are from simulations with at least 64 spheres in the computational domain. The results of simulations with solid volume fractions greater

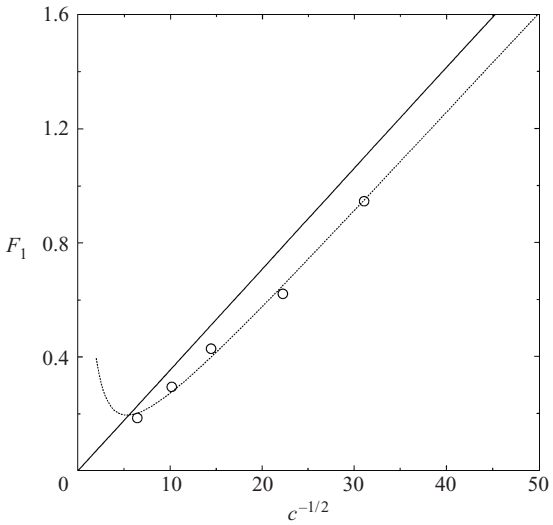

FIGURE 13. The coefficient of the $O(Re^2)$ inertial contribution to the average non-dimensional drag force on the spheres in random arrays as a function of the solid volume fraction. The symbols are from lattice-Boltzmann simulations, the solid line is the $O(c^{-1/2})$ theory (1) of Kaneda (1986), and the dotted line is Kaneda's theory with $O(1)$ and $O(c^{1/2})$ corrections that were obtained from the simulations.

than approximately 0.1 are given to a reasonable approximation by the fit

$$F_1 = 0.110 + 5.10 \times 10^{-4} \exp(11.6c), \tag{48}$$

which is shown as the dotted line in figure 14.

Over the range of Reynolds numbers for which the theory for $Re \ll 1$ is applicable, the inertial contribution to F is considerably smaller than the non-dimensional Stokes-flow drag force, particularly at large solid volume fractions, and hence care must be taken to ensure that the average velocity obtained from the simulations is sufficiently close to steady-state. As shown in § 5, the average velocity at small Reynolds numbers relaxes exponentially at long times. The average velocity used to calculate F was therefore obtained by fitting an exponentially decaying function to the time series of $|\langle \boldsymbol{u} \rangle|$ from the simulations. Since the average drag force is known *a priori*, this gives a more accurate estimate of F, particularly at small Reynolds numbers.

Figure 14 also shows F_1 obtained from the lattice-Boltzmann simulations of Maier *et al.* (1998) (packing P1 in their paper) for flow in a cylindrical randomly packed bed of spheres (square). Despite the order imposed by the walls of the container on the sphere configuration, their simulations are consistent with ours, showing that the drag force at small Reynolds numbers is not significantly affected by the sphere configuration.

Also shown in figure 14 is F_1 obtained from the experimental results of Fand *et al.* (1987) (cross). As explained in the introduction, to obtain this value we assumed a transition from Re^2 to Re scaling, and required that both F and $\partial F/\partial Re$ be continuous there. With these assumptions, their experimental results suggest that $F1 = 0.92$, which is in good agreement with the simulations at the relatively large solid volume fraction of 0.643.

Similarly to simple cubic arrays, F_1/F_0 decays monotonically with increasing solid volume fraction, consistent with the fact that F_1 is very difficult to measure at large

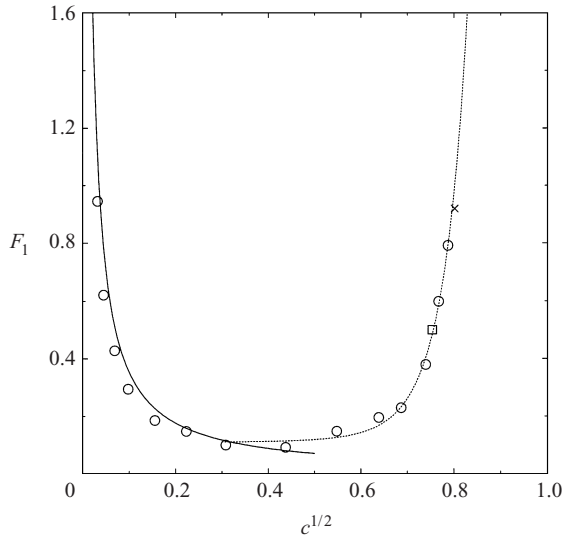

FIGURE 14. The coefficient of the $O(Re^2)$ inertial contribution to the average non-dimensional drag force on the spheres in random arrays as a function of the solid volume fraction: ○, our lattice-Boltzmann simulations, the solid line is the $O(c^{-1/2})$ theory (1) of Kaneda (1986), □, the lattice-Boltzmann simulations of Maier *et al.* (1998) for flow in a cylindrical randomly packed bed of spheres. ×, the experiments of Fand *et al.* (1987), and the dotted line is a fit (48) to the results of our lattice-Boltzmann simulations with $c > 0.1$.

solid volume fractions. Physically, these results show that because fluid inertia is manifested at distances furthest from the spheres, the hydrodynamic interactions at large solid volume fractions are indeed dominated by the effects of viscosity, and hence the first effects of fluid inertia are most significant at very small solid volume fractions.

7. Summary

The lattice-Boltzmann method has been used to examine the effects of fluid inertia on flows in fixed ordered and random arrays of spheres. Steady flows with small but finite Reynolds numbers were considered, as well as unsteady flows whose Reynolds number was practically zero. The results bridge the gap between the extensive literature that exists on Stokes flows in porous media and the moderate-Reynolds-number flows addressed in the accompanying paper (Hill *et al.* 2001).

In the case of unsteady flows with zero Reynolds number, the fluid was accelerated from rest toward a steady Stokes flow. The hydrodynamic force on the spheres at short and long times was shown to be dominated by quasi-steady drag and added-mass forces, and hence the Basset history force could be neglected, to a reasonable approximation. The added-mass coefficient was obtained from a potential-flow approximation for short times and a quasi-steady viscous-flow approximation for long times. The temporal evolution of the average velocity and drag force predicted by this simple theory were in excellent agreement with simulations.

Next, steady flows with small but finite Reynolds numbers were examined. At all solid volume fractions, the first inertial contribution to the non-dimensional drag force was found to be proportional to the square of the Reynolds number, as predicted by the theory of Mei & Auriault. Consequently, when the Reynolds number is sufficiently

small, the inertial correction to the Stokes flow drag force on the spheres in both ordered and random arrays increases with the cube of the average velocity.

The theory developed for dilute simple cubic arrays of spheres required matching the periodic fundamental solution of the Oseen equations to the solution of the Stokes equations for flow past a single sphere in an unbounded fluid. It accurately captured the dependence of the drag force on the solid volume fraction and the direction of the flow relative to the axes of the arrays. Simulations showed that the first inertial correction to the Stokes-flow drag force is most significant at very small solid volume fractions, because the Stokes-flow drag force at large solid volume fractions increases much more rapidly with the solid volume fraction than the inertial correction.

When the Reynolds number based on the sphere separation is large, but the Reynolds number based on the sphere radius is still small, the first inertial contribution to the non-dimensional drag force on the spheres is proportional to the Reynolds number, as expected from Oseen's theory for a single sphere in an unbounded fluid. Our theory and simulations show that inertial corrections to the drag force in this dilute limit may be accounted for, to a reasonable approximation, by neglecting inertial hydrodynamic interactions beyond the Oseen approximation.

Finally, simulations were found to be in good agreement with Kaneda's theory for dilute random arrays of spheres when the Reynolds number based on the Brinkman screening length is small. The behaviour at large solid volume fractions is qualitatively the same as for ordered arrays.

This work was funded by the National Science Foundation (NSF) under grant number CTS-9526149, and the computations were performed using the resources of the Cornell Theory Center. We would also like to thank Alexander Z. Zinchenko for providing the close-packed random sphere configurations used in this work.

REFERENCES

Andrade, J. S., Almeida, M. P., Mendes Filho, J., Havlin, S., Suki, B. & Stanley, H. E. 1997 Fluid flow through porous media: The role of stagnant zones. *Phys. Rev. Lett.* **79**, 3901–3904.

Batchelor, G. K. 1967 *An Introduction to Fluid Dynamics*. Cambridge University Press.

Bevington, P. R. & Robinson, D. K. 1992 *Data Reduction and Error Analysis for the Physical Sciences*. McGraw-Hill.

Brinkman, H. C. 1947 A calculation of the viscous force exerted by a flowing fluid on a dense swarm of particles. *Appl. Sci. Res.* A **1**, 27–34.

Carman, P. C. 1937 Fluid flow through a granular bed. *Trans. Inst. Chem. Engrs Lond.* **15**, 150–156.

Chen, S. & Doolen, G. D. 1998 Lattice Boltzmann method for fluid flows. *Ann. Rev. Fluid Mech.* **30**, 329–364.

Cheng, H. & Papanicolaou, G. 1997 Flow past periodic arrays of spheres at low Reynolds number. *J. Fluid Mech.* **335**, 189–212.

Childress, S. 1972 Viscous flow past a random array of spheres. *J. Chem. Phys.* **56**, 2527–2539.

Clift, R., Grace, J. R. & Weber, M. E. 1978 *Bubbles, Drops, and Particles*. Academic.

Durlofsky, L. & Brady, J. F. 1987 Analysis of the Brinkman equation as a model for flow in porous media. *Phys. Fluids* **30**, 3329–3341.

Edwards, D. A., Shapiro, M., Bar-Yoseph, P. & Shapira, M. 1990 The influence of Reynolds number upon the apparent permeability of spatially periodic arrays of cylinders. *Phys. Fluids* A **2**, 45–55.

Eidsath, A., Carbonell, R. G. S., Whitaker, S. & Herrmann, L. R. 1983 Dispersion in pulsed systems – iii. Comparison between theory and experiments for packed beds. *Chem. Engng Sci.* **38**, 1803–1816.

Fand, R. M., Kim, B. Y. K., Lam, A. C. C. & Phan, R. T. 1987 Resistance to the flow of fluids

through simple and complex porous media whose matrices are composed of randomly packed spheres. *Trans. ASME: J. Fluids Engng* **109**, 268–274.

Ghaddar, C. K. 1995 On the permeability of unidirectional fibrous media: A parallel computational approach. *Phys. Fluids* **7**, 2563–2586.

Hasimoto, H. 1959 On the periodic fundamental solution of the Stokes equations and their application to viscous flow past a cubic array of spheres. *J. Fluid Mech.* **5**, 317–328.

Hill, R. J. 2001 The effects of fluid inertia on flows in porous media. PhD thesis, Cornell University.

Hill, R. J., Koch, D. L. & Ladd, A. J. C. 2001 Moderate-Reynolds-number flows in ordered and random arrays of spheres. *J. Fluid Mech.* **448**, 243–278.

Hinch, E. J. 1977 An averaged-equation approach to particle interactions in a fluid suspension. *J. Fluid Mech.* **83**, 695–720.

Howells, I. D. 1974 Drag due to the motion of a Newtonian fluid through a sparse random array of small fixed rigid objects. *J. Fluid Mech.* **64**, 449–475.

Kaneda, Y. 1986 The drag on a sparse random array of fixed spheres in flow at small but finite Reynolds number. *J. Fluid Mech.* **167**, 455–463.

Kim, S. & Russel, W. B. 1985 Modelling of porous media by renormalization of the Stokes equations. *J. Fluid Mech.* **154**, 269–286.

Koch, D. L. 1990 Kinetic theory for a monodisperse gas-solid suspension. *Phys. Fluids* A **2**, 1711–1723.

Koch, D. L. & Brady, J. F. 1985 Dispersion in fixed beds. *J. Fluid Mech.* **154**, 399–427.

Koch, D. L. & Ladd, A. J. C. 1997 Moderate Reynolds number flows through periodic and random arrays of aligned cylinders. *J. Fluid Mech.* **349**, 31–66.

Koch, D. L. & Sangani, A. S. 1999 Particle pressure and marginal stability limits for a homogeneous monodisperse gas fluidized bed: Kinetic theory and numerical simulations. *J. Fluid Mech.* **400**, 229–263.

Ladd, A. J. C. 1990 Hydrodynamic transport coefficients of random dispersions. *J. Chem. Phys.* **93**, 3484–3494.

Ladd, A. J. C. 1994*a* Numerical simulations of particulate suspension via a discretized Boltzmann equation. Part 1. Theoretical foundation. *J. Fluid Mech.* **271**, 285–309.

Ladd, A. J. C. 1994*b* Numerical simulations of particulate suspension via a discretized Boltzmann equation. Part 2. Numerical results. *J. Fluid Mech.* **271**, 311–339.

Maier, R. S., Kroll, D. M., Kutovsky, Y. E., Davis, H. T. & Bernard, R. S. 1998 Simulation of flow through bead packs using the lattice-Boltzmann method. *Phys. Fluids* **10**, 60–74.

Mei, C. C. & Auriault, J. L. 1991 The effect of weak inertia on flow through a porous medium. *J. Fluid Mech.* **222**, 647–663.

Perry, R. H. & Green, D. 1984 *Perry's Chemical Engineers' Handbook*. McGraw Hill.

Rojas, S. & Koplik, J. 1998 Nonlinear flow in porous media. *Phys. Rev.* E **58**, 4776–4782.

Rothman, D. H. & Zaleski, S. 1997 *Lattice-Gas Cellular Automata*. Cambridge University Press.

Sangani, A. S. & Acrivos, A. 1982 Slow flow through a periodic array of spheres. *Intl J. Multiphase Flow* **8**, 343–360.

Sangani, A. S., Zhang, D. Z. & Prosperetti, A. 1991 The added mass, Basset, and viscous drag coefficients in nondilute bubbly liquids undergoing small-amplitude oscillatory motion. *Phys. Fluids* A **3**, 2955–2970.

Verberg, R. & Ladd, A. J. C. 2000 A lattice-boltzmann model with sub-grid scale boundary conditions. *Phys. Rev. Lett.* **84**, 2148–2151.

Zick, A. A. & Homsy, G. M. 1982 Stokes flow through periodic arrays of spheres. *J. Fluid Mech.* **115**, 13–26.

Zinchenko, A. Z. 1994 Algorithm for random close packing of spheres with periodic boundary conditions. *J. Comput. Phys.* **114**, 298–306.